Multiscale Finite Element Modeling of Sheet Molding Compound (SMC) Composite Structure based on Stochastic Mesostructure Reconstruction

Zhangxing Chen[1,2,†], Tianyu Huang[3,†], Yimin Shao[1], Yang Li[2], Hongyi Xu[2,*], Katherine Avery[2], Danielle Zeng[2], Wei Chen[3], Xuming Su[2]

1. State Key Laboratory of Mechanical Transmission, Chongqing University, Chongqing, China, 400044

2. Research and Advanced Engineering, Ford Motor Company, Dearborn, MI, United States, 48121

3. Northwestern University, Evanston, IL, United States, 60201

† These authors contribute equally to this work

* Corresponding author: Dr. Hongyi Xu, hxu41@ford.com

Abstract

Predicting the mechanical behavior of the chopped carbon fiber Sheet Molding Compound (SMC) due to spatial variations in local material properties is critical for the structural performance analysis but is computationally challenging. Such spatial variations are induced by the material flow in the compression molding process. In this work, a new multiscale SMC modeling framework and the associated computational techniques are developed to provide accurate and efficient predictions of SMC mechanical performance. The proposed multiscale modeling framework contains three modules. First, a stochastic algorithm for 3D chip-packing reconstruction is developed to efficiently generate the SMC mesoscale Representative Volume Element (RVE) model for Finite Element Analysis (FEA). A new fiber orientation tensor recovery function is embedded in the reconstruction algorithm to match reconstructions with the target characteristics of fiber orientation distribution. Second, a metamodeling module is established to improve the computational efficiency by creating the surrogates of mesoscale analyses. Third, the macroscale behaviors are predicted by an efficient multiscale model, in which the spatially varying material properties are obtained based on the local fiber orientation tensors. Our approach is validated through experiments at both meso- and macro-scales, such as tensile tests assisted by Digital Image Correlation (DIC) and mesostructure imaging.

Keywords: SMC; multiscale; RVE; mesostructure reconstruction; orientation tensor

1. Introduction

To meet the increasingly strict vehicle emission regulations, chopped carbon fiber sheet molding compounds (SMC) are considered as a promising candidate lightweight material for the mass-produced vehicle components [1]. However, design of automobile components remains challenging due to the difficulties in predicting the spatially varying, anisotropic mechanical properties of SMC. Previous studies have shown that local properties of SMC are strongly influenced by the complex material flow patterns during the compression molding process [2]. To resolve this issue, a multiscale modeling approach needs to be developed to account for the heterogeneous mesostructures of SMC.

A great number of works have been done on developing multiscale modeling approaches for random fiber reinforced composite materials. The first category is the micromechanics-based analytical method, which is based on the concept of Eshelby tensor [3]. In this category, the Mori-Tanaka method [4, 5] and the self-consistent method [6, 7] laid the foundation of the analysis of the properties of random fiber reinforced composites. For example, Tandon and Weng [8] predicted the elastic properties of random oriented composites based on the Mori-Tanaka method by considering the variation of average stress in the matrix. Chen et al. [9] derived explicit formulae of the elastic moduli of the aligned and randomly oriented composites based on the Mori-Tanaka method. Miloh et al. [10] developed a generalized self-consistent method for evaluation of the random oriented composites. Advani and Tucker [11] introduced the fiber orientation tensor and developed a tensor averaging technique to predict the mechanical properties of random oriented composites. Such methodology was later extended to different types of injection molded short fiber composites, as in the works by Gupta and Wang [12] and the works by Tseng et al. [13]. Although proven to be successful in predicting macroscale elastic properties, this method is limited in

capturing spatial variations in microstructure, or the nonlinear properties including material damage evolution [14, 15] .

The second category is the Finite Element Analysis (FEA)-based computational micromechanical methods [14], which include both micro-/meso- and macro-scale models. At the micro-/meso- scale, FEA models are established for micro-/meso- structures to predict the homogenized local material properties. The homogenized properties are then passed to the macro-scale FEA models as inputs to simulate the mechanical behavior of the components. For example, Gudes and Kikuchi [16] developed a FEA based homogenization method to determine the effective elastic constants of general composites with the consideration of microstructural features. To further improve the prediction accuracy, the adaptive finite element method has been developed. Ghosh et al. [17-20] developed a Voronoi cell-based finite element model to investigate the mechanical properties of heterogeneous media. Harper [21-23] developed a random fiber chip Representative Volume Element (RVE) models to simulate the mechanical properties of random fiber composites. Although the predictive capability is improved by incorporating the microstructure/mesostructure into the model, significant computational costs are usually inevitable. Therefore, a cost efficient multiscale modeling method is needed for predicting the mechanical behaviors of chopped carbon fiber SMC.

Micro-/meso- structure reconstruction is a key component of multiscale modeling of composite materials. The goal is to generate digital material structures based on material characteristics for further analysis of properties or performance, e.g. via FEA simulations. In general, the reconstruction algorithms start with fiber geometry statistics, which include, but are not limited to, fiber orientation distributions, fiber size and aspect ratio, and fiber volume fraction. Fibers or fiber bundles are often approximated with simple mathematical objects such as rods or

rectangles. The objects are then packed into a predefined space to build the RVE. Since the reconstruction process starts from fiber statistics, it is desirable to generate statistically equivalent RVEs for simulations and statistical analysis of properties/performance.

The most popular approaches for random discontinuous fiber composite reconstruction are the random sequential adsorption (RSA)-based packing algorithms [15, 24-33]. RSA methods pack objects sequentially into a space with random locations while avoiding the new object overlapping existing ones until a desired number of objects are packed or a pre-specified number of iterations is reached [34]. After RSA was first introduced as a packing scheme for simulating the protein molecules adsorption onto solid surfaces [34], Evans and Ferrar [24] studied the packing of fibers, focusing on investigating the effect of different parameters such as in-plane angle and aspect ratio on the fiber volume fraction. Since then, RSA-based models have been widely used for the RVE analysis. To mimic the true geometry of the composite, some new variants of this approach were developed for more complicated reconstructions, including packing fibers with different aspect ratios [27] or orientation distributions [30], packing fiber bundles instead of single fibers [21-23], and allowing curved fibers [1, 15, 21, 22]. RSA methods are generally fast, but they assume a completely random fiber orientation state and the fiber volume fraction of the RVEs can hardly exceed 60%.

Other packing schemes include the Monte Carlo method [35], which packs fibers with random configurations first, and then perturbs their locations and angles to make the system reach a desired orientation state while avoiding overlapping. Williams and Philipse studied packing of fibers through simulating the mechanical contraction phenomenon [36]. Dirrenburger applied the Poisson process to generate large random fiber models [37]. However,

these techniques were still developed for low fiber volume fraction cases. Furthermore, all but the Monte Carlo method simply assumes a purely random distribution of fiber orientation.

In recent developments, Li et al [30] proposed a new method, which extracts the geometry information of fiber bundles from optical microscopic images and generates the mesostructure with Voronoi tessellation. Each Voronoi cell represents a local area of unidirectional fibers, which is the unique feature of SMC composites' mesostructure. Since the fibers are not modeled explicitly, RVEs with arbitrary volume fractions and orientation states could be reconstructed this way. However, the 2D Voronoi cell-based reconstruction cannot fully capture the 3D geometry of the fiber tow, so the method is not suitable for simulations of nonlinear and failure behavior. Therefore, a new reconstruction algorithm is needed to generate RVEs with high volume fraction (70% - 80%), pre-defined orientation state (not necessarily completely random) obtained from other sources such as the process simulation, and it should explicitly model the chip-like fiber bundles.

In order to address the aforementioned issues, an improved multiscale framework and the associated techniques are proposed to predict the mechanical behaviors of chopped carbon fiber SMC. This framework is featured by three new developments. First, a stochastic mesostructure reconstruction algorithm is developed for reconstructing the high-volume fraction SMC mesostructures. The input statistical mesostructure characteristic (fiber orientation tensor) is obtained from the compression molding simulations. To reduce the error in recovering the fiber orientation distribution function from the fiber orientation tensor, a new recovery function is proposed. Second, the Kriging metamodel is employed to reduce the computational cost of mesoscale material property evaluation in the multiscale modeling process. Third, a multiscale modeling framework is developed to connect the mesostructure models to the macroscale simulations. The proposed framework enables the rapid prediction of

SMC properties considering the spatial variations in local material properties via the use of mesoscale metamodels. The rest part of the paper is organized as follows: Section 2 introduces a multiscale modeling framework and covers four major topics: overview of the multiscale framework (Section 2.1), compression molding simulation for generating the fiber orientation tensor (Section 2.2), metamodeling of SMC mesoscale material properties (Section 2.3), and integration in the macroscale FEA model (Section 2.4). Section 3 first introduces a chip-packing mesostructure reconstruction algorithm and a new fiber orientation distribution recovery function (Section 3.1). In addition, Section 3.2 introduces the mesoscale FEA model and metamodeling of SMC mesoscale material properties. In Section 4, the computational predictions are validated experimentally by the Digital Image Correlation (DIC) tensile bar tests and the SMC mesostructure images. The prediction errors are also examined in this section. Section 5 is the summary of this work.

2. Multiscale Modeling Framework for SMC Chopped Carbon Fiber Composites Structure

This section introduces the proposed multiscale modeling framework. The inputs of this framework include the geometrical parameters of fiber tows, the given material properties of fiber and matrix, and the compression modeling process parameters. Outputs are the predicted the macroscale elasticity.

2.1 Overview

The compression molding process of an SMC part is illustrated in Figure 1 (upper left corner). The initial charge containing chopped carbon fiber chips, uncured resin, and curing agent. The initial charge is preheated and placed in the designed positions in the mold cavity. During the compression molding process, the initial charge is compressed and cured under certain pressure and temperature. Driven by the compression force, the flow of fiber chips and resin fills the cavity to form the desired geometry. The flow pattern has a strong impact on the orientation

of the fiber chips at different locations. The local fiber orientation distributions consequently determine the local mesostructure features and local material properties of the formed SMC part.

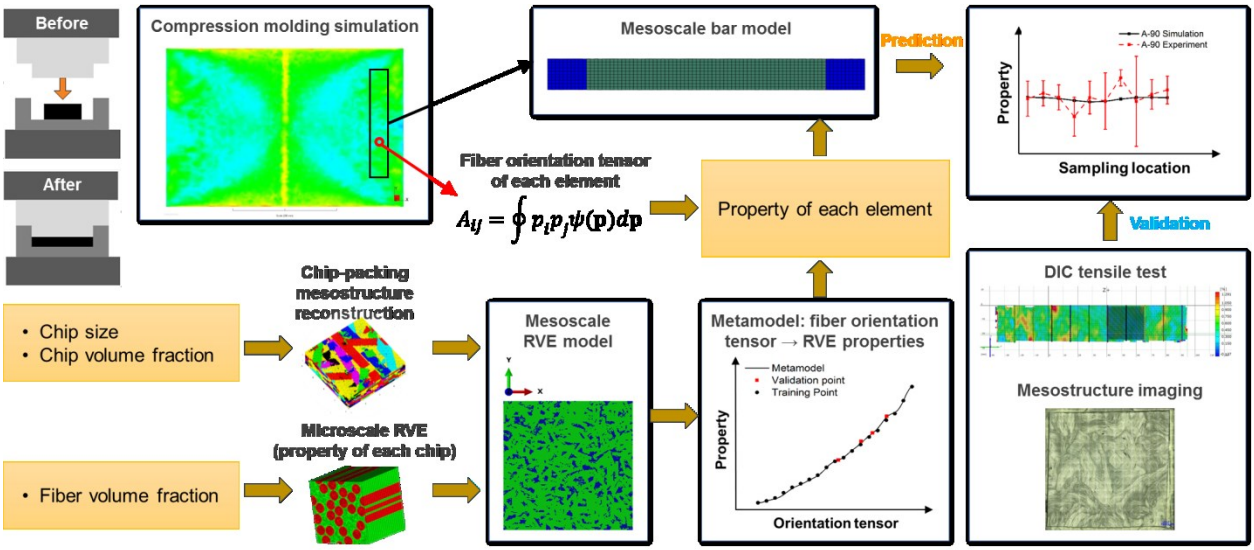

Figure 1: Multiscale modeling and validation framework for chopped carbon fiber SMC structure

In order to predict the structure performance with consideration of variations in local material properties, a multiscale modeling framework is proposed (Figure 1). This framework consists of three critical modules: (1) Compression molding simulation, which predicts the spatial distribution of fiber orientation tensor over the entire component; (2) Mesostructure property analysis, which generates a metamodel that establishes the relation between the fiber orientation and the material properties. The SMC mesostructure RVE is reconstructed based on the statistical fiber orientation information (Section 3), and the training data of the metamodel are generated by conducting FEA on the mesostructure RVE models; (3) Macroscale FEA model, which predicts the macroscale mechanical behavior of a part by integrating local properties obtained from the fiber orientation-property metamodel. The predictions of material properties are validated by experiments, which are introduced in Section 4.

2.2 Compression molding simulation: prediction of the fiber orientation tensor

The fiber orientation at a given point can be completely defined by a fiber orientation Probability Density Function (PDF). However, a PDF cannot be directly used in numerical simulations of complex geometries because it is verbose and difficult to use in the flow molding simulation [38, 39]. Therefore, the fiber orientation tensor is developed as a simplification of the PDF. Only the even-order tensors are of interest since the odd-order fiber orientation tensors are equal to zero. Currently, the fiber orientation tensor, particularly the second and fourth orders of the tensor, is widely used in the existing molding process simulation tools (e.g. Autodesk Moldflow). Notating the fiber orientation tensor matrix by $\boldsymbol{A}$, the second order and fourth order fiber orientation tensors are defined as [11]:

$$A_{ij} = \oint p_i p_j \psi(\mathbf{p}) d\mathbf{p} \tag{1}$$

$$A_{ijkl} = \oint p_i p_j p_k p_l \psi(\mathbf{p}) d\mathbf{p} \tag{2}$$

where p_i are the components of the unit vector $\mathbf{p}$ describing the direction of a single fiber and $\psi(\mathbf{p})$ is the fiber orientation PDF. The PDF can be recovered once the fiber orientation tensors are known [11]:

$$\psi(\mathbf{p}) = \frac{1}{4\pi} + \frac{15}{8\pi} b_{ij} f_{ij}(\mathbf{p}) + \frac{315}{32\pi} b_{ijkl} f_{ijkl}(\mathbf{p}) + \mathrm{K} \quad , \tag{3}$$

where b_{ij},$b_{ijkl}$are the deviatoric fiber orientation tensors:

$$b_{ij} = A_{ij} - \frac{1}{3}\delta_{ij} \tag{4}$$

$$\delta_{ij} = \begin{cases} 0, & i \neq j \\ 1, & i = j \end{cases} \tag{5}$$

$$\begin{aligned} b_{ijkl} = A_{ijkl} &- \frac{1}{7}(\delta_{ij}A_{kl} + \delta_{ik}A_{jl} + \delta_{il}A_{jk} + \delta_{jk}A_{il} + \delta_{jl}A_{ik} + \delta_{kl}A_{ij}) \\ &+ \frac{1}{35}(\delta_{ij}\delta_{kl} + \delta_{ik}\delta_{jl} + \delta_{il}\delta_{jk}) \end{aligned} \quad , \tag{6}$$

and f_{ij} , f_{ijkl} are tensor basis functions of $\mathbf{p}$:

$$f_{ij}(\mathbf{p}) = p_i p_j - \frac{1}{3}\delta_{ij} \tag{7}$$

$$f_{ijkl}(\mathbf{p}) = p_i p_j p_k p_l - \frac{1}{7}(\delta_{ij} p_k p_l + \delta_{ik} p_j p_l + \delta_{il} p_j p_k + \delta_{jk} p_i p_l + \delta_{jl} p_i p_k + \delta_{kl} p_i p_j) + \frac{1}{35}(\delta_{ij}\delta_{kl} + \delta_{ik}\delta_{jl} + \delta_{il}\delta_{jk}) \tag{8}$$

The fiber orientation tensor of a part is predicted using the reactive compression molding module in Autodesk Moldflow. Details of compression molding experiments and simulations are presented in [40] and briefly reviewed hereafter. Following the parameters used in the compression molding experiments, the dimension of the cavity is set to 457.2 mm×304.8 mm×1.2 mm, while the dimension of the initial charge is 152.4 mm×152.4 mm×8 mm. The mold temperature is set to 150°C. The peak press force during the molding is 1500 kN. A layered tetrahedron mesh is generated following the default meshing procedure in Moldflow, with an in-plane mesh size of ~5 mm and the number of meshed layers as 14 for both the cavity and the initial charge. The output fiber orientation tensors are extracted from Moldflow and then mapped to the tensile bar FEA models, which simulate the performances of the samples that are cut on different locations from the plaque. Due to thermal flow and the effect of part geometry, the fiber orientation tensor differs from element to element in the tensile bar model.

2.3 Mesostructure property analysis: metamodeling of the relation between the fiber orientation tensor and the elastic property using the mesostructured RVE model

A chip-packing based RVE model is developed to predict the mechanical properties of SMC mesostructures. Based on the stochastic reconstructions of SMC mesostructures, FEA models are established to simulate SMC material properties (details in Section 3). There are two phases in the SMC mesostructure: pure resin, and fiber

tows (chips) that contain both aligned fibers and resin. The resin properties are provided by the material supplier, and the chopped fiber chip's properties are predicted from a microscale RVE model. In our previous work, an RVE model has been established for the unidirectional (UD) fiber composites following the procedure in [41]. This UD RVE model is leveraged to predict the fiber tows' material properties, because all the fibers are aligned to the same direction inside each fiber tow. The inputs of the UD RVE model include resin properties and fiber properties. The predicted fiber tow properties are considered as material constants in the mesostructure RVE model.

Metamodels of the mesoscale RVE are created and used in predicting material properties at each integration point in the macroscale FEA model. The inputs of the RVE model include the fiber orientation tensor and other mesostructure geometrical parameters (e.g. chip size, volume fraction V_F. More details of the RVE modeling process will be introduced in Section 3. The outputs (response) of the metamodels contain all entries of the stiffness matrix obtained from FEA simulation. For the compressed chopped fiber SMC, the Z component of the fiber chip's orientation is negligible compared to the X and Y components. Therefore, the fiber orientation distribution of the SMC component can be described by a 2D fiber orientation tensor for simplification. If the second-order 2D fiber orientation tensor is represented as A_{ij}, the relation between the principal and non-principal orientation matrix is expressed as:

$$\mathrm{a}_{mn} = R_{mi} R_{nj} A_{ij}, \tag{9}$$

where R_{mi} are the entries of the rotation matrix, a_{mn} are the entries of the principal orientation tensor matrix, and A_{ij} are the entries of the non-principal orientation tensor matrix.

In the last step of simulation, the stiffness matrix of the original non-principal tensor matrix is obtained by transforming the principal stiffness matrix back to the non-principal space. The transformation formula between the non-principal and the principal stiffness matrices is:

$$C_{ijkl}=R_{mi}R_{nj}R_{pk}R_{ql}C_{mnpq} \quad , \tag{10}$$

where $R_{mi}, R_{nj}, R_{pk}, R_{ql}$ are the components of the rotation matrix, C_{ijkl} and C_{mnpq} are the output stiffness matrices of the RVE models with inputs A_{ij} and a_{ij} respectively. According to the definition of A_{ij} given in [11]:

$$A_{11} + A_{22} = a_{11} + a_{22} = 1 \tag{11}$$

any 2D principal orientation tensor can be fully represented by a single parameter a_{11}. The relation between the principal orientation tensor and the property of interest can thus be established by a 1D metamodel with single input of a_{11}. The training points of the metamodel are generated with equal distance (0.05) in the range of $a_{11} \in$[0.05, 0.95]. The outputs of the metamodeling step are 21 components of the stiffness matrix in Voigt form, hence 21 metamodels are established in total. In addition, four validation points a_{11}= [0.52, 0.66, 0.72, 0.82] are generated to check the prediction accuracy of the metamodels.

Kriging [42-44] is selected as the technique for metamodeling. The Kriging model is expressed as:

$$\mathrm{y} = \sum_{j=1}^{k} \beta_j f_j(x) + Z(x), \tag{12}$$

where β_j is the weighted coefficient, $f_j(x)$ is a known fixed function and $Z(x)$is a Gaussian process model. In the training process, the hyperparameters of the Gaussian process model are determined by the Maximum Likelihood Estimation (MLE). The trained Kriging models are used to predict the stiffness matrix components when a new a_{11} value is provided. In Figure 2, plots of Kriging metamodels are provided for the four in-plane

components of the stiffness matrix, where good accuracy is observed. According to the prediction values of the validation points, the maximum prediction error of all Kriging metamodels is below 2.65%.

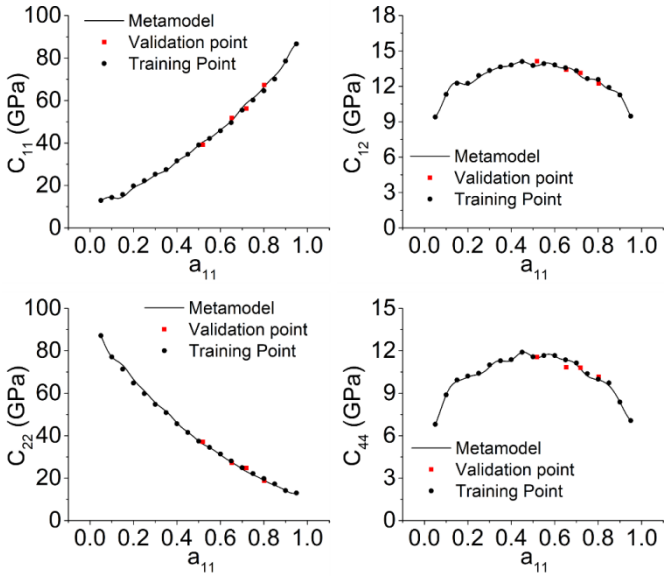

Figure 2: The relationship between a_{11} and the in-plane components of the stiffness matrix

2.4 Macroscale modeling: prediction of the structure properties based on mesoscale properties

The macroscale FEA modeling process is demonstrated using the tensile bar example. A macroscale tensile bar model (Figure 3) is set up in Abaqus/Standard to simulate the mechanical performances of the samples cut from different locations on a molded SMC plaque. The mesh is generated using C3D8R solid elements. The dimension of the model is set as the same as the real experimental samples (more details will be provided in Section 4.2.2). The fiber orientation tensors differ from element to element in the tensile bar models. In this study, the fiber orientation tensors of the plaque part are extracted from the compression molding simulation results in Moldflow [40] and then mapped to the macro-scale tensile bar FEA model in Abaqus/Standard. With the fiber orientation tensor as the input, the anisotropic stiffness matrix of each element in the tensile bar model is obtained by the Kriging metamodels. A virtual tensile bar test is conducted using the macroscale FEM model (Figure 3). The boundary

conditions (BC) of a uni-axial tensile test are applied to the meshed structure. On the right gripping area, a displacement is applied in the axial direction and all the other degrees of freedom are constrained. On the left gripping area, all degrees of freedom are constrained. The simulation outs the stress and strain fields, which are used to calculate the tensile modulus of the entire bar and the tensile modulus of a local region.

Figure 3: Macroscale bar model. The BCs are applied to each node in the gripping area

3. SMC Mesostructure Modeling based on a Chip Packing Reconstruction Algorithm

Stochastic reconstruction of SMC mesostructure is the foundation of the mesoscale RVE simulation, a critical component of the proposed multiscale modeling framework. This section provides details of the proposed chip packing reconstruction algorithm and the FEA model of the mesostructure RVE.

3.1 Chip packing mesostructure reconstruction algorithm

A stochastic chip packing algorithm is developed to generate SMC mesotructure reconstructions of a high fiber tow volume fraction. The reconstructed structure matches the target geometrical statistics, such as the average fiber tow size, fiber tow volume fraction and the fiber tow orientation distribution.

3.1.1 Overview

The RVE is reconstructed by packing rectangular chips into a 3D voxelated flat cuboid space. The input parameters include the size of the chips and the plates, the target orientation tensor, and the target volume fraction. The details of inputs and outputs are summarized in Table 1. The outputs are the coordinates of the voxels of each chip and the chip orientation, information needed for FEA modeling.

Table 1: List of the SMC Reconstruction Inputs

Description		Parameter
From manufacturer's setting	Plate width	W_P
	Number of the layers	n_P
	Chip width	W_C
	Chip length	L_C
	Chip Volume Fraction	V_F
From molding simulation	RVE Orientation Tensor Matrix	$\boldsymbol{A}$

Let **V** be a 3D voxel space with size $W_P \times W_P \times n_P$. A voxel has a set of coordinates (i, j, k), and for each voxel $\mathbf{V}(\mathbf{i},\mathbf{j},\mathbf{k})$:

$$\mathbf{V}(\mathbf{i},\mathbf{j},\mathbf{k}) = \begin{cases} 0 & \text{if } \mathbf{V}(\mathbf{i},\mathbf{j},\mathbf{k}) \text{ is a resin voxel} \\ n & \text{if } \mathbf{V}(\mathbf{i},\mathbf{j},\mathbf{k}) \text{ is a chip voxel belonging to the n}^{th} \text{ chip} \end{cases} \quad (13)$$

A chip's location is represented by the coordinate of its center point. Packing of the n-th chip includes finding a feasible location in **V** for the chip, determining the set of voxels assigned to it, and making appropriate adjustments of voxels if overlapping between chips is detected. Figure 4 depicts the flowchart of the algorithm.

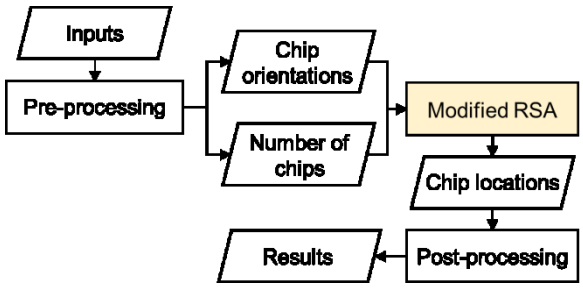

Figure 4: Information flow of the reconstruction algorithm

In this algorithm, chip orientations and the number of chips per layer are first determined in the pre-processing step. Next, chips are packed one-by-one and layer-by-layer under a modified RSA scheme until the desired number

of chips is satisfied. Finally, fine tuning is performed and the reconstructed structure is exported for FEA modeling. The details of each step of the algorithm will be discussed in the following sections.

3.1.2 Pre-processing

The pre-processing process includes estimation of the number of chips and generation of chip orientations. The number of chips in a layer is estimated based on the information of chip and plate sizes and the target chip volume fraction. Denoting the numbers of the chips in a layer and in total by N_L and N_T respectively, they are estimated by

$$N_L = \left\lceil \frac{W_P^2 \cdot V_F}{W_C \cdot L_C} \right\rceil. \qquad (14)$$
$$N_T = N_L \cdot n_P$$

Note that since the estimated number of chips can only be an integer and the volume fraction after packing all chips will not exactly match the target in most cases. Therefore, the post-processing step is necessary to ensure that a target volume fraction is met.

The reconstruction procedure described below takes the principal form of fiber orientation tensor as input. For the non-principal orientation tensor, it is first transformed into the corresponding principal form based on Equation (9). After obtaining the stiffness matrix of the correspondent principal tensor, the non-principal stiffness matrix is generated by a transformation back to the non-principal space.

To fully recover the fiber orientation distribution function PDF, theoretically one needs infinite sets of orientation tensors [45]. In reality, the fiber orientation distribution is approximated by truncating the series shown in Equation (5). Higher accuracy of the recovered PDF is expected if the higher order tensor basis functions are involved in Equation (5). We recover the PDF from the 2nd and 4th order tensors since most

simulations keep the 2nd order ones as the orientation state variable and the 4th order tensors can be obtained from the 2nd order tensors using closure approximation methods. There are several closure approximation methods, such as linear closure approximations [45], quadratic closure approximations [45], orthotropic fitted closure approximation (ORF) [12, 46], invariant-based optimal fitting (IBOF) closure approximations [47], etc. This paper employs the IBOF closure approximation. IBOF is more accurate than the linear and quadratic closure approximations, meanwhile it requires less computational time than ORF [47].

Given a 2D principal fiber orientation tensor as the input, the 4th order fiber orientation tensor is obtained through the closure approximation. Then the fiber orientation PDF is recovered following Equations (5-10). However, it is found in the present study that the recovery process shows relatively significant error when fiber chips are highly aligned along a certain direction. To evaluate the accuracy throughout this process, the second order fiber orientation tensor of the recovered PDF is obtained following Equation (1). The recovery error is evaluated as the difference between the original principal second order fiber orientation tensor and the principal second order fiber orientation tensor of the recovered PDF:

$$Err = \frac{\left| a_{11}^{recover} - a_{11}^{input} \right|}{a_{11}^{input}} \times 100\% \tag{15}$$

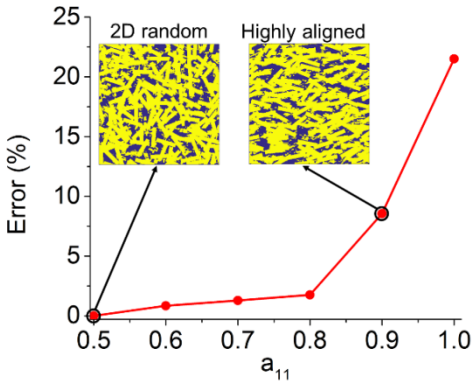

Figure 5: Error of the IBOF recovery function

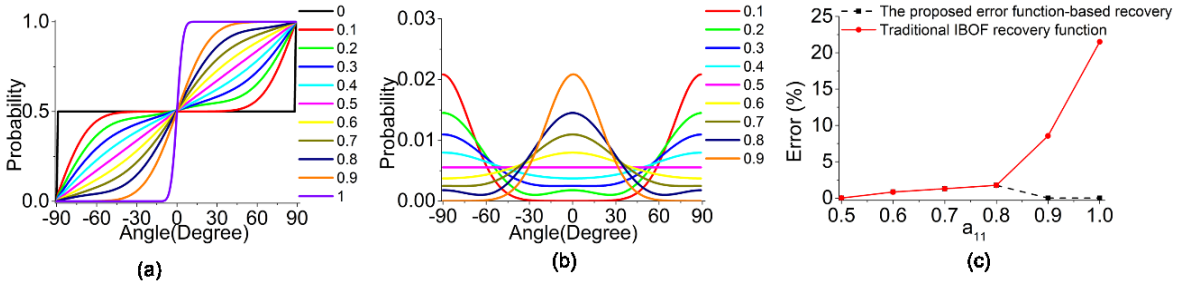

Figure 6: CDF and PDF of the fiber orientation distribution represented by the Gauss error function, and the errors of the orientation tensor recovery functions. (a) CDF of different a_{11}; (b) PDF of different a_{11} without 0 and 1 case; (c) Comparison of recover error

In Figure 5, it is shown that the error increases significantly when a_{11} (the input principal orientation tensor) exceeds 0.8 (chips are strongly aligned to one direction). To reduce the error, we propose a modified recovery procedure, in which the Gauss error function is used to represent the fiber orientation Cumulative Density Function (CDF) for the highly aligned cases. The new recovery function is separated into two parts. For the relatively random orientation distributions ($0.2 \leq a_{11} \leq 0.8$), we still adopt the IBOF closure approximation as it is sufficiently accurate. For the highly aligned distributions ($a_{11} > 0.8$ and $a_{11} < 0.2$), the proposed Gauss error function-based recovery is used:

$$CDF = \begin{cases} \dfrac{1}{2\sqrt{\pi}} \displaystyle\int_{-x/K(a_{II})}^{x/K(a_{II})} e^{-x^2} dx + \frac{1}{2} & a_{II} > 0.8 \\ \displaystyle\int_{-90}^{x} \psi(x) dx & 0.8 \geq a_{II} \geq 0.2 \\ \dfrac{1}{2\sqrt{\pi}} \displaystyle\int_{-(x-90)/K(a_{II})}^{(x-90)/K(a_{II})} e^{-x^2} dx + \frac{1}{2} & a_{II} < 0.2 \end{cases}, \quad (16)$$

where the range of x is $[-90^\circ, 90^\circ)$, and it represents the direction of a fiber chip. For 2D fiber chip reconstructions, in-plane angles are sufficient to describe the chip directions. Therefore, $\psi(\mathbf{P})$ in Equation (3) can be reduced as $\psi(x)$, a function of the in-plane chip angle. The parameter K is a function of a_{II}. The

$K(a_{11})$ values are determined using gradient-based optimization, which minimizes the difference between the original a_{11} and the a_{11} of the recovered PDF. The recovered CDFs of different a_{11} values are plotted in Figure 6 (a) and the corresponding PDFs are plotted in Figure 6 (b). The error of the recovered PDF is plotted in Figure 6 (c). Compared to the IBOF closure approximation, the modified fiber orientation recovery function significantly reduces the recovery error for the highly aligned fiber tow distributions.

3.1.3 Modified-RSA (MRSA)

Though RSA can be a useful scheme for SMC RVE reconstruction [15, 24-30], the upper limit of the volume fraction that can be achieved by the conventional RSA of equilateral rectangles (squares) is reported to be 56.2% [34], and the value drops with the increase of the chip aspect ratio. However, in our RVE reconstruction problem, the target volume fraction (around 80%) is much higher than the limit and the chips' aspect ratio is around 5:1. Therefore, the algorithm needs to be modified to achieve a higher volume fraction.

The modified-RSA algorithm for multi-layer voxelated systems is illustrated in Figure 7. In this algorithm, the feasibility condition for candidate chip locations and the treatment for overlapping chips are altered. Compared to the conventional RSA, in which a candidate location is rejected simply because a chip on that location will intersect with one or more chips on the plate, the feasibility condition is relaxed in our approach so that at most two chips can intersect at one location and the overlapping part can rise to the upper layer.

After a feasible location is found for a chip, a process called "Rise or Sink" will be applied to each of the chip voxels. The process mimics the situation that when a chip is laid above another one with a different orientation, the unsupported chip segment will sink down while the overlapping part will remain on the top, which creates curved chips.

3.1.4 Post-processing and volume fraction tuning

"Rise and Sink" is a chip segment reallocation process: for a plate where the packing is going on, it dynamically moves chip segments to upper and lower layers to increase the space utilization. Note when packed layer-by-layer, the chips on the very bottom layer will not undergo the "sink" process. This leads to a much higher volume fraction of the first layer as chip segments will not leave it by sinking. Also note that there will be always one more layer than desired since an additional layer will be created to receive the rising chip segments from the top layer. These two phenomena suggest that to obtain an RVE with steady volume fractions across layers, it is necessary to generate a thicker reconstruction having extra layers, while only layers in the middle with consistent volume fractions will be used to form the RVE.

The last step is to fine tune the reconstructed structure to match the target volume fraction exactly. To achieve this goal, some chips are selected randomly and their boundaries are expanded by one unit until the overall volume faction is close enough to the target.

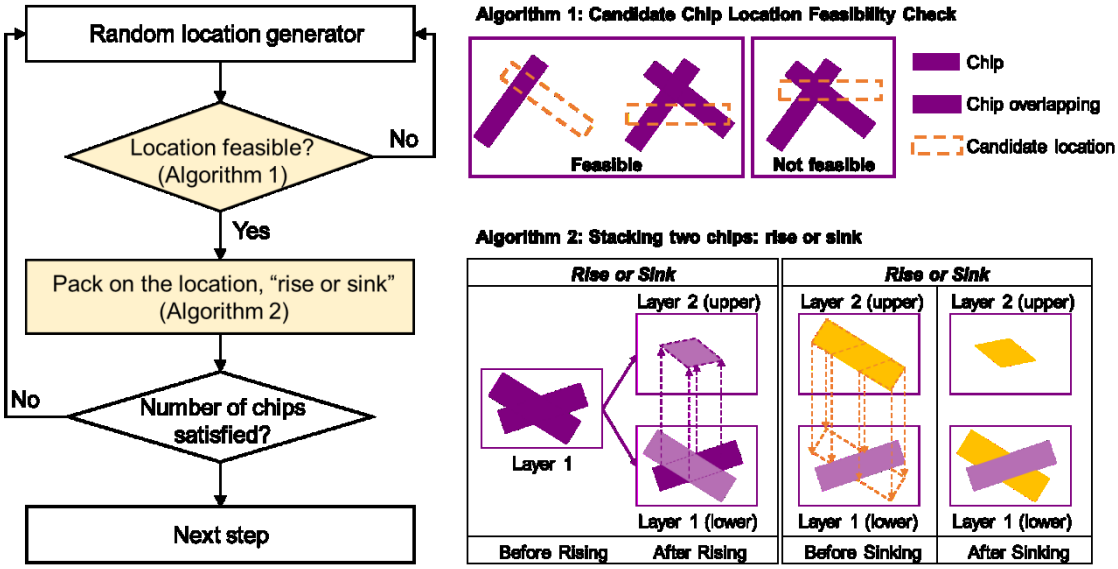

Figure 7: Flowchart of MRSA

3.1.5 Results

An reconstruction for an isotropic randomly oriented SMC is generated using parameters in Table 2:

Table 2: Pre-specified Input Parameters

Name	Value
Volume fraction	0.8
Chip size	50 mm×10 mm
Plate size	300 mm×300 mm
Layers	4
Orientation Tensor	$\begin{bmatrix} 0.5 & 0 \\ 0 & 0.5 \end{bmatrix}$

The four reconstructed layers and their corresponding volume fractions are plotted in Figure 8. To test the algorithm's performance with different inputs, reconstructions with different orientation tensors, volume fractions and chip sizes are compared with the setting in Figure 8 and Table 2. Figure 9 shows good agreement between the reconstruction targets and results.

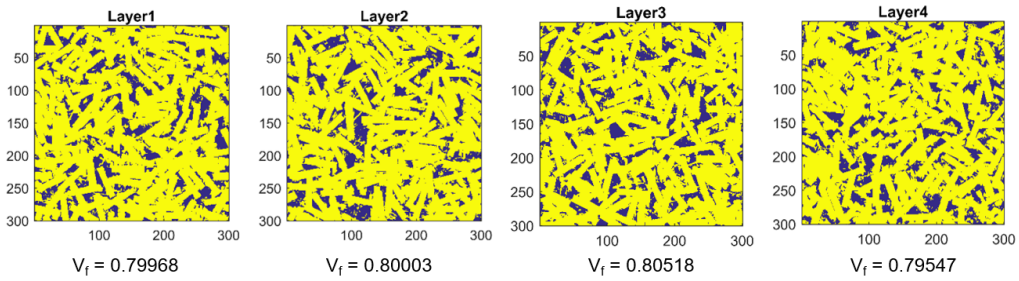

Figure 8: Illustration of a 4-layer Reconstruction

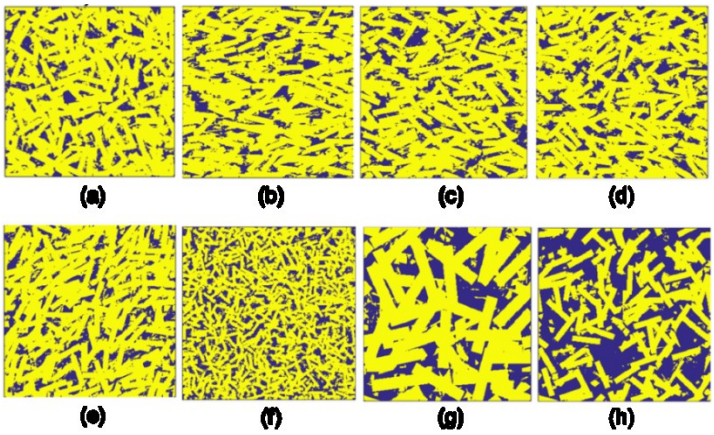

Figure 9: RVE in Different Settings. (a) Original Setting as in Table 2, (b) Orientation Tensor $=\begin{bmatrix}1 & 0\\0 & 0\end{bmatrix}$; (c) Orientation Tensor $=\begin{bmatrix}0.8 & 0\\0 & 0.2\end{bmatrix}$; (d) Orientation Tensor $=\begin{bmatrix}0.7 & 0\\0 & 0.3\end{bmatrix}$; (e) Orientation Tensor $=\begin{bmatrix}0.5 & 0.5\\0.5 & 0.5\end{bmatrix}$; (f) Chip Size = 25×5; (g) Chip size = 100×20; (h) Volume Fraction = 0.5

3.2 Mesostructure FEA model based on the reconstructions

The FEA models are built by taking the voxelated chip packing reconstructions as inputs. Each voxel in the reconstruction is converted into a C3D8R solid element in Abaqus/Standard. Each element is assigned with the corresponding mechanical properties. Material orientations of fiber chip elements are defined so that the 1-axis in the local coordinate system is aligned in the direction of fibers in the chip. Figure 10 (a) shows an in-plane view of an FEA model of a SMC reconstruction. Figure 10 (b) shows the 3D view of the FEA model. Elements in green are fiber chip elements while the ones in blue are elements of matrix resin. An example of the material orientation for a set of elements belonging to a single chip is shown in Figure 10 (c). The material parameters are listed in Table 3.

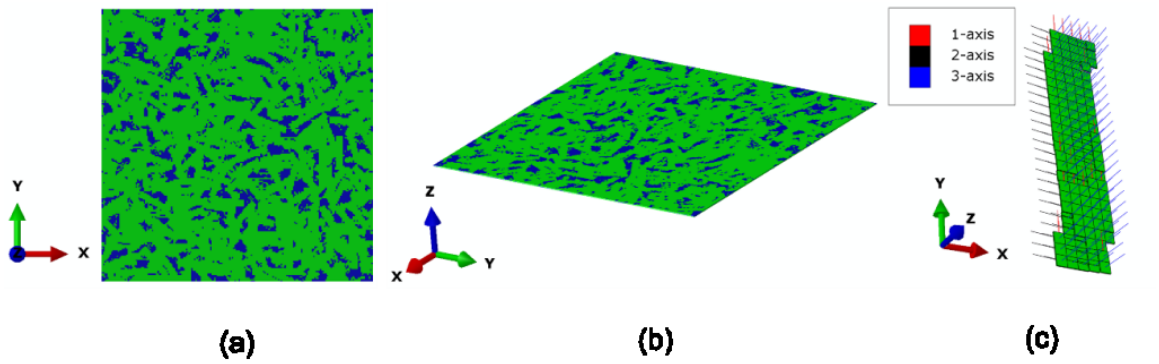

Figure 10: FEA model of a SMC reconstruction and the geometry of a meshed chip. (a) In-plane view of an FEA model of a SMC reconstruction; (b) 3D view of the FEA model; (c) Geometry and orientation of a meshed chip

3.3 Determination of the RVE size based on sensitivity studies

An RVE represents a domain in the material that is large enough to contain sufficient micro-features so that the domain's microstructure statistics and properties are spatially invariant [48-50]. Due to limited computational resources, it is impossible to use an infinitely large RVE to predict the material properties. Therefore, a trade-off exists between the prediction accuracy and computational time. Given the size of the fiber chips (the size of the microstructure features), sensitivity studies are conducted to determine the minimal RVE size that is statistically representative. The RVE size is finally determined as 200 mm×200 mm×0.8 mm by the following procedure:

(1) Given a trial RVE thickness, conduct a convergence study on the relation between the in-plane size and the simulated properties to determine a proper in-plane size;

(2) Fix the in-plane size as the value determined in the previous step, conduct a convergence study on the relation between the thickness and the simulated properties to determine a proper thickness.

More details about the sensitivity study are provided in the Appendix.

Table 3: Fiber chip and resin properties

Fiber chip				Resin	
E_{11} (GPa)	125.9	μ_{12}	0.32	E (GPa)	3.8

E_{22} (GPa)	8.6	μ_{13}	0.32	μ	0.38
G_{12} (GPa)	4.8				

4. Experimental Validation of the Multiscale Simulation Results

4.1 Experiment setup and results

Plaques of 457.2 mm × 304.8 mm × 1.2 mm are manufactured by compression molding [40] under the same processing condition. Initial charges with dimensions of 152.4mm × 152.4mm × 8mm are placed at the center of the cavity. Testing samples are cut from each plaque at selected locations as shown in Figure 11. The elastic moduli of the tensile bar samples are obtained by the DIC tensile test, and the fiber orientation tensors at the selected locations are measured using microscopic image analysis.

4.1.1 Measurement of elastic modulus by DIC test

Tensile bar samples are cut at five locations A, B, C, D, E to measure the mechanical properties at different flow lengths, and multiple tests were conducted at each sampling location. As shown in Figure 11, the samples are cut in both 0 and 90 degree orientations in order to measure elastic properties along different directions. Since the initial charge is placed in the center of the cavity [50], the flow pattern is considered as centrosymmetric, i.e., the properties at location B (D) are assumed to be equivalent to those at location C (E).

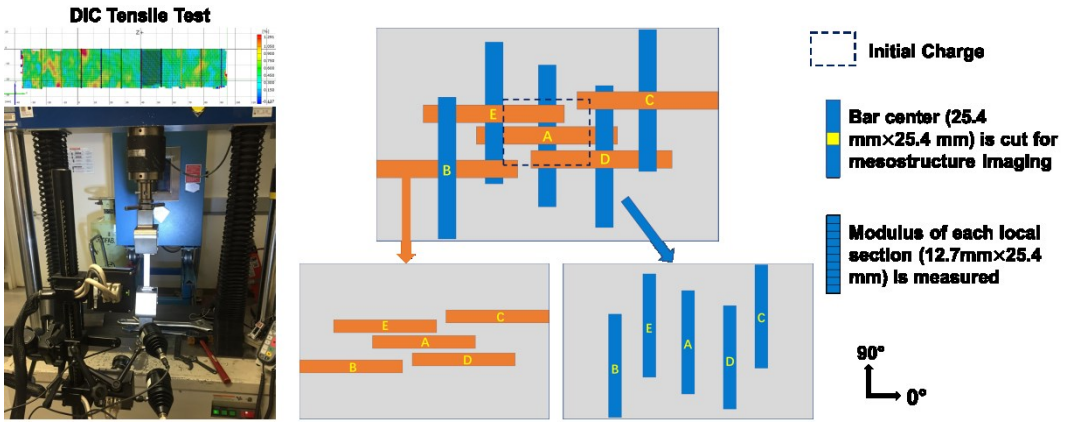

Figure 11: DIC tensile tests on the SMC tensile bar samples that are cut from the molded plaque

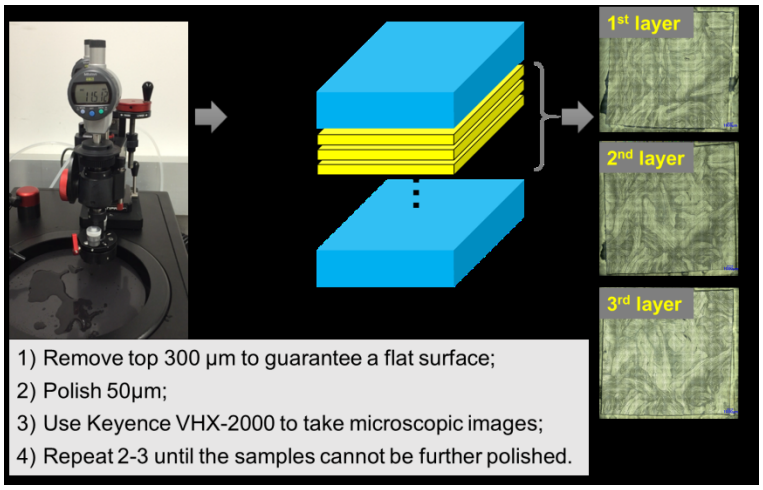

Figure 12: Mesostructure characterization procedure

The tensile test procedure follows the ASTM standard D3039/D3039M. Displacement control mode is used, and the loading speed is set as 2 mm/min. DIC system is used to record the strain field of the tensile bar. Both material properties and the fiber orientation distributions are obtained from this experiment. First, the modulus of the specimen's central area (25.4 mm×25.4 mm) is obtained based on the strain measured by DIC. After the DIC tests, the central area of the bar is cut off for mesostructure imaging using optical microscope (Section 4.1.2). The fiber orientation tensors obtained from image analysis are used to validate the compression molding simulation. It is also used as the input of the mesoscale RVE simulation, the results of which are compared to the measured elastic properties to validate the accuracy of the RVE model. Second, the elastic moduli of several smaller sections (12.7mm×25.4 mm) are calculated over the entire length of the DIC measurement area. The modulus of each section is used to validate the prediction of the multiscale model.

4.1.2 Mesostructure Characterization

The fiber orientation tensor of a sample is obtained by image analysis on optical microscope images of the polished sample surface. A series of mesostructure images are taken in the through thickness direction. Standard metallographic procedures are employed to remove material layer by layer. An automated polishing machine (MultiPrepTM System 15-2000-Gl produced, Allied High Tech Products, Inc.) is used to remove a layer of material with a thickness of ~50 μm. The mesostructure characterization procedure is shown in Figure 12. The number of sample images obtained for regions A, B and E is 14, 10 and 16, respectively. To characterize the fiber orientation tensor from the mesostructure image, a MATLAB image analysis package is developed based on a computer vision algorithm which is originally used for fingerprints analysis [51, 52]. In Table 4, the measured and the simulated fiber orientation tensor matrices are compared.

Table 4: Fiber orientation tensor for different locations

Location	Measured T_m (mean fiber orientation tensor)	Predicted T_m (mean fiber orientation tensor)
A	$\begin{bmatrix} 0.646 & 0.06 \\ 0.06 & 0.354 \end{bmatrix}$	$\begin{bmatrix} 0.610 & -0.02 \\ -0.02 & 0.390 \end{bmatrix}$
B	$\begin{bmatrix} 0.552 & -0.03 \\ -0.03 & 0.448 \end{bmatrix}$	$\begin{bmatrix} 0.570 & -0.05 \\ -0.05 & 0.430 \end{bmatrix}$
E	$\begin{bmatrix} 0.560 & -0.03 \\ -0.03 & 0.440 \end{bmatrix}$	$\begin{bmatrix} 0.575 & -0.01 \\ -0.01 & 0.425 \end{bmatrix}$

4.2 Validation of the model predictions

4.2.1 Experimental validation of the predicted mesoscale RVE properties

Mesoscale RVE models are established to predict the elastic properties of the SMC material with given fiber orientation tensors. As the purpose is to study the accuracy of the RVE model, the experimentally measured orientation tensor is used as input. The simulated fiber orientation tensors are not used in the validation of RVE models since there are errors in compression molding simulations. The chip size is set as 25.4 mm×5 mm×1.2 mm

and the fiber volume fraction is 41.1% as measured by a burn-off test conducted according to ASTM D3171-99. The volume fraction of fiber chips in the SMC composites is 80%. The properties of the fiber chip (calculated from a UD RVE [41]) and the pure resin serve as the simulation inputs. At each test location, 15 RVE models are generated by the stochastic reconstruction. The predicted elastic modulus E_{11} and E_{22} are compared to the experimental testing results in Figure 13.

Table 5: Input parameters for simulation

		Location A	Location B	Location E
Fiber Tow Properties	Chip size	25.4 mm × 5 mm		
	Chip thickness	~100 um		
	Fiber V_F	41.1%		
	Fiber	A type of commercial carbon fiber		
	Resin	Epoxy		
Fiber orientation tensor		$\begin{bmatrix} 0.646 & 0.06 \\ 0.06 & 0.354 \end{bmatrix}$	$\begin{bmatrix} 0.552 & -0.03 \\ -0.03 & 0.448 \end{bmatrix}$	$\begin{bmatrix} 0.560 & -0.03 \\ -0.03 & 0.440 \end{bmatrix}$

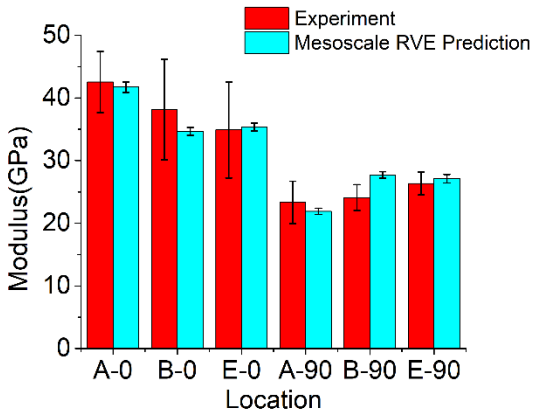

Figure 13: Experimental validation of the mesostructure RVE model (E_{11} and E_{22})

It is observed that the simulated elastic modulus E_{11} and E_{22} match well with the experimental results on locations A and E. At location B, the RVE model overestimates the modulus in the 90-degree direction, and

underestimates the modulus in the 0-degree direction. More discussion of the prediction errors will be provided in Section 4.3.

4.2.2 Experimental validation of the predicted properties of the local sections on the tensile bar

The tensile bar is divided into 10 local sections along the length direction. Using the macroscale model mentioned in Section 2.4, the modulus of each local section is predicted and compared with the experimental data from DIC tensile tests (Figure 14). To validate the proposed multiscale modeling method, the simulated fiber orientation tensors are used in the prediction of the tensor bar properties.

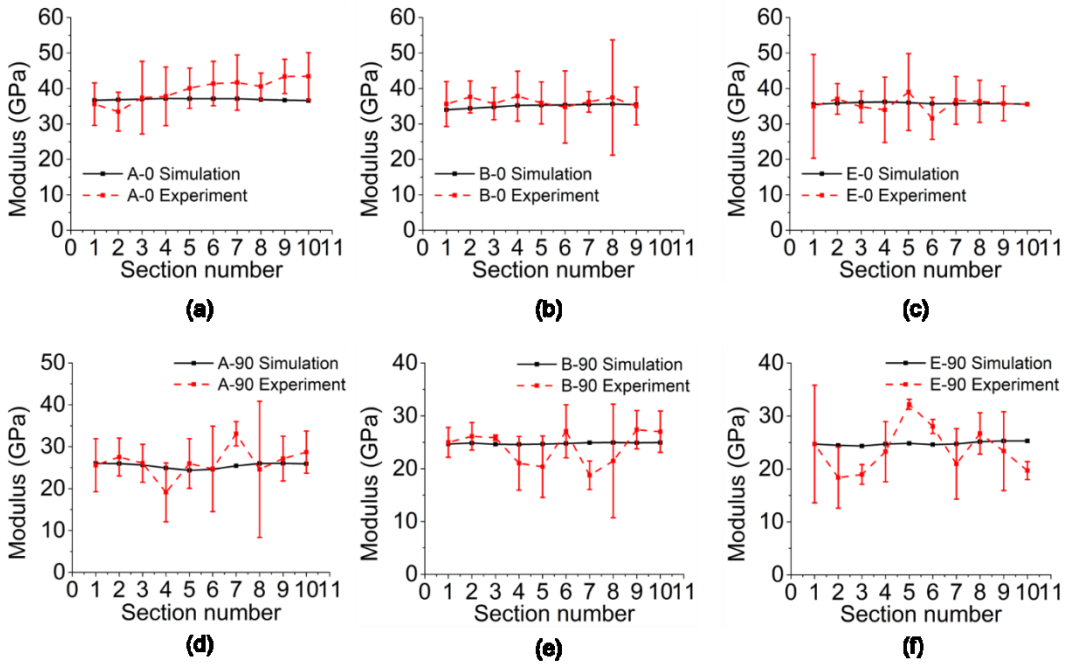

Figure 14: Comparison of local modulus of each section on the tensile bar with the simulation results

In general, a good match is observed between predictions by the multiscale model and the experimental results. Most of the predicted local section moduli are close to the mean of the tested samples. However, we also observe deviations at some locations, which can be explained by the prediction error in fiber orientation tensor by

the compression molding simulation. The spatial variation and the standard deviation of the tensile modulus are significant, especially for the E-90 sample as shown in Figure 14 (f). A continuous flow field simulation may have trouble in capturing such intensive variations in a relatively small region. Furthermore, the effect of the manufacturing process uncertainty, currently not incorporated in the multiscale modeling framework, may play an important role here and therefore requires future efforts.

4.3 Discussion

The prediction errors are contributed by all three models in the multiscale framework. First, a mesoscale RVE model is developed to capture the mesostructure characteristic of the SMC. As we presented in Section 4.2.1, this RVE model can predict the elastic properties at location A and E accurately, but it underpredicts the modulus in the 0-degree direction and overpredicts the modulus in the 90-degree direction at location B (having the longest flow length). The prediction error is induced by the bias in the input fiber orientation tensors. Additionally, due to limitations in the current polishing technique, we cannot measure the fiber orientation tensor near the surfaces of the sample. Therefore, the average of the measured tensors may not be entirely representative of the full thickness. The prediction error is also caused by the use of 2D fiber orientation tensor to reconstruct the 3D mesostructured model. The component on the Z direction (a_{33}) is assumed to be small and neglected in the model.

Second, the Kriging metamodel was established to represent the relation between the fiber orientation tensor and the elastic properties. The maximum prediction error is below 2.65%. The errors from the metamodel may propagate to the final performance predictions. Although we believe that the metamodel is sufficiently accurate, the prediction error can be further reduced by adding more training points.

Third, a multiscale model is established to predict the performance of the tensile bar on the macroscale. To capture the spatial variations in local material properties, the input material property of each element is predicted based on the simulated local fiber orientation tensor. The real local modulus has a large variance that cannot be captured by the macroscale model. Such discrepancies are induced by the errors in the input local fiber orientation tensor. To resolve this issue, it is essential to improve the compression molding simulation for more accurate predictions of the local fiber orientation tensors.

5. Summary

To capture the anisotropic properties of the chopped carbon fiber SMC composites, a multiscale modeling framework is developed based on an integration of mesostructure RVE simulations with the macroscale FEA through metamodeling. This work features several new developments in mesostructure modeling and multiscale information management. First, a stochastic chip-packing mesostructure reconstruction algorithm is developed to generate RVE models of high fiber tow volume fraction and predefined fiber orientation distribution which are not available in previous methods. Second, a new recovery function is developed based on the Gauss error function. This new function significantly reduces the errors in recovering the highly aligned fiber orientation distribution. Third, a Kriging metamodeling strategy is proposed to reduce the computational costs of multiscale analysis. This strategy enables that the local material properties can be assessed accurately and quickly. The proposed multiscale modeling framework is demonstrated by a case study of tensile bar analysis, in which the variations in local material properties are captured based on the material processing information. Experimental tests, tensile tests using DIC and mesostructure imaging, are conducted to validate the predictions. This work provides a useful

Integrated Computational Materials Engineering (ICME) tool for the future developments of complex SMC structures.

The limitations are summarized as future work: First, the out-of-plane orientation tensor a_{33} cannot be captured by the current mesoscale RVE model. Second, propagation of the uncertainties, such as the variation in the local volume fraction, is not considered in the multiscale model. Third, more validations and efforts are needed to extent the framework to simulate the mechanical behavior of parts with complex geometry.

Acknowledgement

This research is supported by Ford Motor Company and US Department of Energy (Award Number: DE-EE0006867). Zhangxing Chen also warmly thanks the support from China Scholarship Council (CSC).

Appendix. Determination of the proper RVE size and thickness

According to the Δ-criterion of uncertainty propagation [49], the ratio between the RVE model's geometric dimension and the microstructure feature's geometric dimension should be sufficiently large in order to guarantee that the RVE model is spatially invariant in microstructure statistics and material properties. In this study, the microstructure feature's geometric dimension is equivalent to the chip size. A convergence study is conducted to search the minimum in-plane size and thickness of the RVE model.

By fixing the thickness as 0.4 mm, multiple groups of RVE models with different in-plane dimension are generated. The value of the in-plane dimension ranges from 100 mm to 350 mm, with an increment of 50 mm. According to the information on the real material, the input chip size is set as 25.4 mm $\times$ 5 mm $\times$ 0.1 mm, and the chip volume fraction of the fiber chips in the reconstructed RVE model is set as 80%. 15 random realizations are reconstructed for each group. The convergence study is conducted for two typical fiber tow dispersion

status: $a = \begin{bmatrix} 0.5 & 0 \\ 0 & 0.5 \end{bmatrix}$ and $a = \begin{bmatrix} 0.9 & 0 \\ 0 & 0.1 \end{bmatrix}$, which correspond to 2D random fiber chip orientation and highly aligned fiber chip orientation, respectively. The material parameters are listed in Table 3.

The results of the convergence study are summarized in Figure A.1. The average E_{11}, E_{22} and G_{12} values of two different fiber orientation tensors are plotted against the RVE size. It is observed that the predicted modulus converges to a certain value when the in-plane size exceeds 150 mm×150 mm. For all in-plane dimensions tested, the Coefficients of Variation (CoV) values are below 6%, which indicates a small variation among different realizations in the same group. With the consideration of the convergence and computational costs, 200mm×200mm is selected for the following studies.

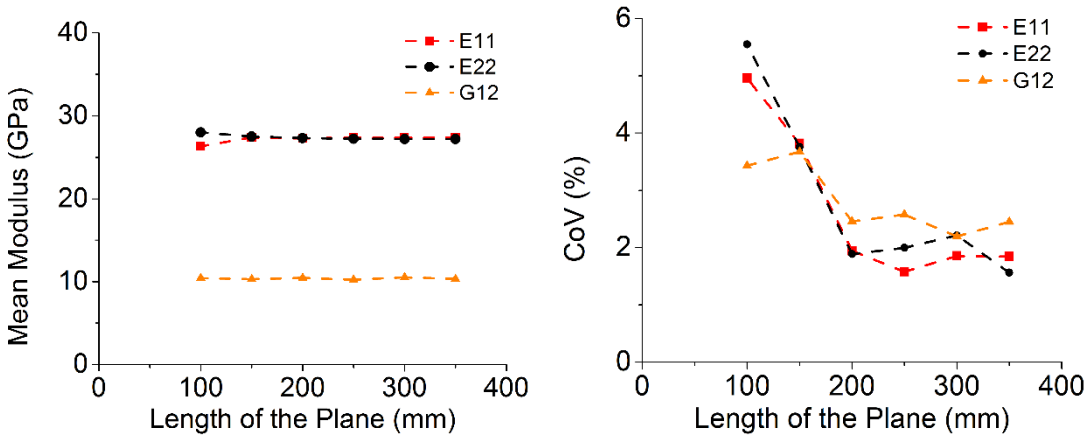

(a) (b)

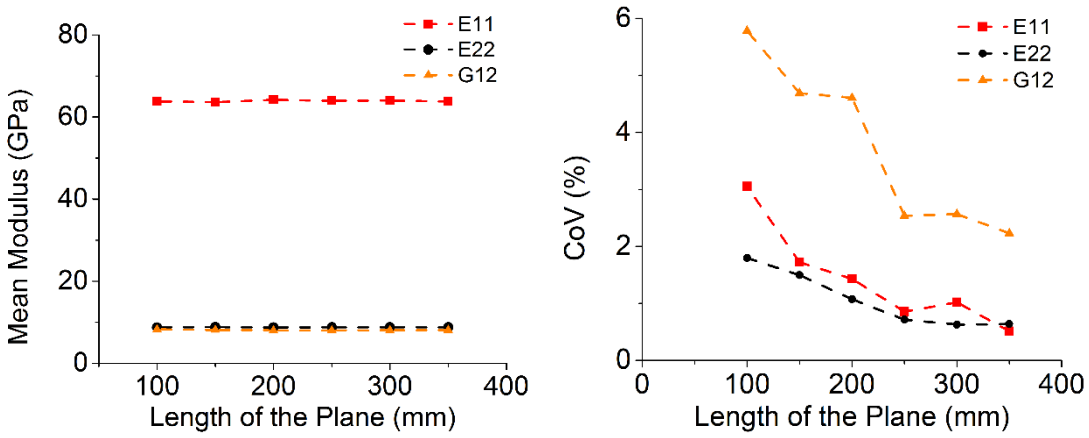

(c) (d)

Figure A.1: Mean modulus (a, c) and CoV (b, d) of E_{11}, E_{22} and G_{12} of RVEs of different plane sizes of fiber orientation tensor $\begin{bmatrix} 0.5 & 0 \\ 0 & 0.5 \end{bmatrix}$ and $\begin{bmatrix} 0.9 & 0 \\ 0 & 0.1 \end{bmatrix}$, respectively.

The thickness of the RVE is another critical factor that influences the simulated properties. Similarly, a convergence study is conducted by fixing the in-plane size of the RVE model. For each thickness, 15 realizations are reconstructed to calculate the mean and CoV of the modulus. The relations between the plane thickness and the mean modulus E_{11}, E_{22} and G_{12} are plotted in Figure A.2. When the thickness increases, the modules converge to a certain value (E_{11} and E_{22} converges to 31.2 (69.4) GPa and G_{12} converges to 11.7 (8.21) GPa for $a = \begin{bmatrix} 0.5 & 0 \\ 0 & 0.5 \end{bmatrix}$ $\left(\begin{bmatrix} 0.9 & 0 \\ 0 & 0.1 \end{bmatrix}\right)$ case). The CoVs of the sample properties are below 5% regardless of the thickness, which indicates a negligible variation among the RVE samples of the same thickness. Finally, the RVE size is determined as 200 mm×200 mm×0.8 mm.

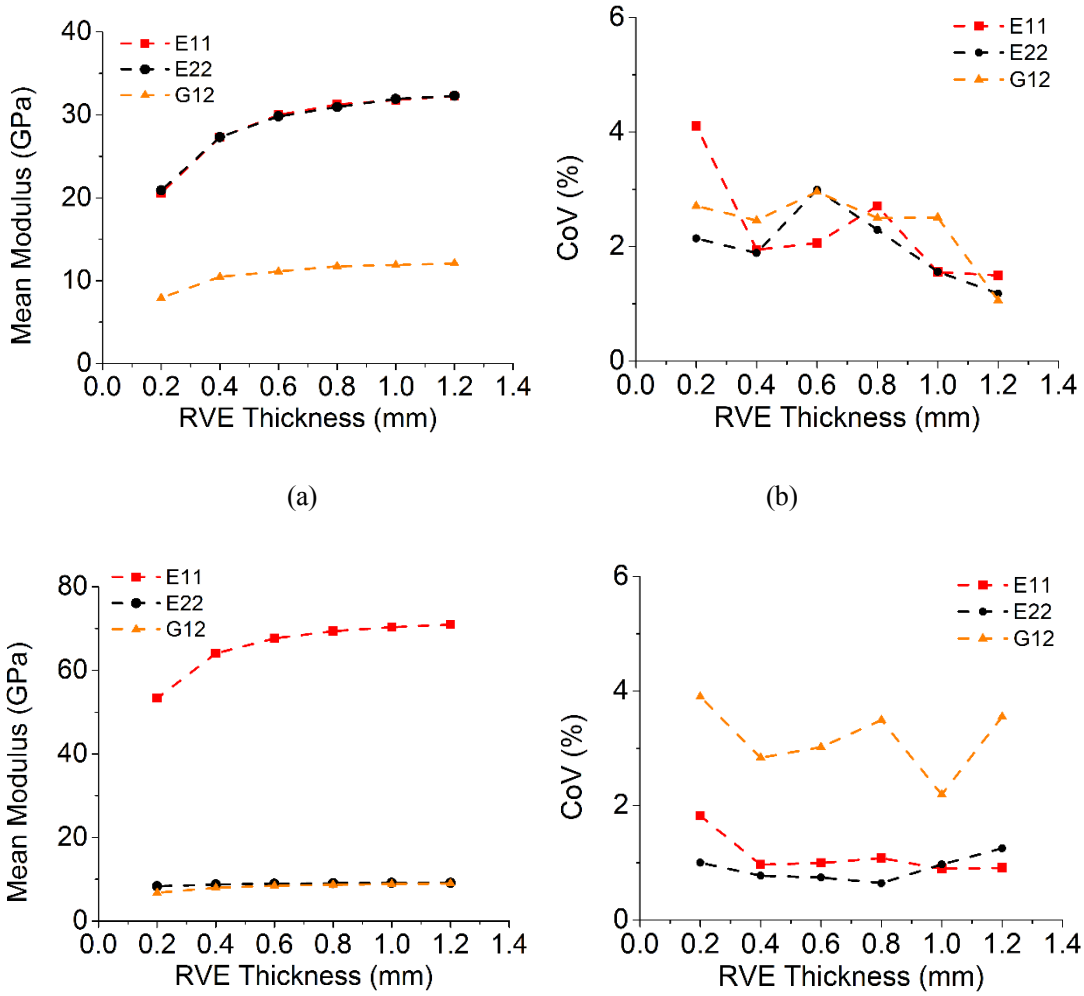

Figure A.2: Mean modulus (a, c) and CoV (b, d) of E_{11}, E_{22} and G_{12} of RVEs of different layers of fiber orientation tensor $\begin{bmatrix} 0.5 & 0 \\ 0 & 0.5 \end{bmatrix}$ and $\begin{bmatrix} 0.9 & 0 \\ 0 & 0.1 \end{bmatrix}$, respectively.

Reference

[1] Pan Y, Iorga L, Pelegri AA. Numerical generation of a random chopped fiber composite RVE and its elastic properties. Composites Science and Technology. 2008;68:2792-8.

[2] Li Y, Chen W, Jin X, Xu H. 3D representative volume element reconstruction of fiber composites via orientation tensor and substructure features. Proceedings of the American Society for Composites - 31st Technical Conference, ASC 20162016.

[3] Eshelby JD. The determination of the elastic field of an ellipsoidal inclusion, and related problems. Proceedings of the Royal Society of London A: Mathematical, Physical and Engineering Sciences: The Royal Society; 1957. p. 376-96.

[4] Benveniste Y. A new approach to the application of Mori-Tanaka's theory in composite materials. Mechanics of materials. 1987;6:147-57.
[5] Mori T, Tanaka K. Average stress in matrix and average elastic energy of materials with misfitting inclusions. Acta metallurgica. 1973;21:571-4.
[6] Hill R. A self-consistent mechanics of composite materials. Journal of the Mechanics and Physics of Solids. 1965;13:213-22.
[7] Budiansky B. On the elastic moduli of some heterogeneous materials. Journal of the Mechanics and Physics of Solids. 1965;13:223-7.
[8] Tandon G, Weng G. Average stress in the matrix and effective moduli of randomly oriented composites. Composites Science and Technology. 1986;27:111-32.
[9] Chen T, Dvorak GJ, Benveniste Y. Mori-Tanaka estimates of the overall elastic moduli of certain composite materials. Journal of applied mechanics. 1992;59:539-46.
[10] Miloh T, Benveniste Y. A generalized self-consistent method for the effective conductivity of composites with ellipsoidal inclusions and cracked bodies. Journal of Applied Physics. 1988;63:789-96.
[11] Advani SG, Tucker III CL. The use of tensors to describe and predict fiber orientation in short fiber composites. Journal of Rheology. 1987;31:751-84.
[12] Gupta M, Wang K. Fiber orientation and mechanical properties of short-fiber-reinforced injection-molded composites: Simulated and experimental results. Polymer Composites. 1993;14:367-82.
[13] Tseng HC, Chang RY, Hsu CH. Accurate predictions of orientation dependent modulus in short-fiber-reinforced composite with experimental validation. Polymer Composites. 2017.
[14] Kwon YW, Allen DH, Talreja R. Multiscale modeling and simulation of composite materials and structures: Springer, 2008.
[15] Pan Y. Stiffness and progressive damage analysis on random chopped fiber composite using FEM: Rutgers The State University of New Jersey-New Brunswick, 2010.
[16] Guedes J, Kikuchi N. Preprocessing and postprocessing for materials based on the homogenization method with adaptive finite element methods. Computer Methods in Applied Mechanics and Engineering. 1990;83:143-98.
[17] Ghosh S, Lee K, Moorthy S. Multiple scale analysis of heterogeneous elastic structures using homogenization theory and Voronoi cell finite element method. International Journal of Solids and Structures. 1995;32:27-62.
[18] Ghosh S, Moorthy S. A Voronoi cell finite element model for random heterogeneous media. Probabilities and Materials: Springer; 1994. p. 273-84.
[19] Lee K, Ghosh S. Small deformation multi-scale analysis of heterogeneous materials with the Voronoi cell finite element model and homogenization theory. Computational Materials Science. 1996;7:131-46.
[20] Ghosh S, Lee K, Moorthy S. Two scale analysis of heterogeneous elastic-plastic materials with asymptotic homogenization and Voronoi cell finite element model. Computer Methods in Applied Mechanics and Engineering. 1996;132:63-116.
[21] Luchoo R, Harper L, Warrior N, Dodworth A. Three-dimensional numerical modelling of discontinuous fibre composite architectures. Plastics, Rubber and Composites. 2011;40:356-62.
[22] Harper L, Qian C, Luchoo R, Warrior N. 3D geometric modelling of discontinuous fibre composites using a force-directed algorithm. Journal of Composite Materials. 2017;51:2389-406.

[23] Harper L, Turner T, Warrior N, Rudd C. Characterisation of random carbon fibre composites from a directed fibre preforming process: The effect of tow filamentisation. Composites Part A: Applied Science and Manufacturing. 2007;38:755-70.
[24] Evans K, Ferrar M. The packing of thick fibres. Journal of Physics D: Applied Physics. 1989;22:354.
[25] Tu S-T, Cai W-Z, Yin Y, Ling X. Numerical simulation of saturation behavior of physical properties in composites with randomly distributed second-phase. Journal of Composite Materials. 2005;39:617-31.
[26] Berger H, Kari S, Gabbert U, Rodríguez Ramos R, Bravo Castillero J, Guinovart Díaz R. Evaluation of effective material properties of randomly distributed short cylindrical fiber composites using a numerical homogenization technique. Journal of Mechanics of Materials and Structures. 2007;2:1561-70.
[27] Kari S, Berger H, Gabbert U. Numerical evaluation of effective material properties of randomly distributed short cylindrical fibre composites. Computational Materials Science. 2007;39:198-204.
[28] Iorga L, Pan Y, Pelegri A. Numerical characterization of material elastic properties for random fiber composites. Journal of Mechanics of Materials and Structures. 2008;3:1279-98.
[29] Pan Y, Iorga L, Pelegri AA. Analysis of 3D random chopped fiber reinforced composites using FEM and random sequential adsorption. Computational Materials Science. 2008;43:450-61.
[30] Li Y, Chen W, Jin X, Xu H. 3D Representative Volume Element Reconstruction of Fiber Composites via Orientation Tensor and Substructure Features. Proceedings of the American Society for Composites: Thirty-First Technical Conference2016.
[31] Qi L, Tian W, Zhou J. Numerical evaluation of effective elastic properties of composites reinforced by spatially randomly distributed short fibers with certain aspect ratio. Composite Structures. 2015;131:843-51.
[32] Tian W, Qi L, Zhou J, Liang J, Ma Y. Representative volume element for composites reinforced by spatially randomly distributed discontinuous fibers and its applications. Composite Structures. 2015;131:366-73.
[33] Liu H, Zeng D, Li Y, Jiang L. Development of RVE-embedded solid elements model for predicting effective elastic constants of discontinuous fiber reinforced composites. Mechanics of materials. 2016;93:109-23.
[34] Feder J. Random sequential adsorption. Journal of Theoretical Biology. 1980;87:237-54.
[35] Gusev A, Heggli M, Lusti HR, Hine PJ. Orientation averaging for stiffness and thermal expansion of short fiber composites. Advanced Engineering Materials. 2002;4:931-3.
[36] Williams S, Philipse A. Random packings of spheres and spherocylinders simulated by mechanical contraction. Physical Review E. 2003;67:051301.
[37] Dirrenberger J, Forest S, Jeulin D. Towards gigantic RVE sizes for 3D stochastic fibrous networks. International Journal of Solids and Structures. 2014;51:359-76.
[38] Han K-H, Im Y-T. Numerical simulation of three-dimensional fiber orientation in short-fiber-reinforced injection-molded parts. Journal of materials processing technology. 2002;124:366-71.
[39] Folgar F, Tucker III CL. Orientation behavior of fibers in concentrated suspensions. Journal of Reinforced Plastics and Composites. 1984;3:98-119.
[40] Li Y, Chen Z, Xu H, Dahl J, Zeng D, Mirdamadi M, et al. Modeling and Simulation of Compression Molding Process for Sheet Molding Compound (SMC) of Chopped Carbon Fiber Composites. SAE International Journal of Materials and Manufacturing. 2017;10:130-7.

[41] Melro A, Camanho P, Pinho S. Generation of random distribution of fibres in long-fibre reinforced composites. Composites Science and Technology. 2008;68:2092-102.
[42] Booker AJ, Dennis JE, Frank PD, Serafini DB, Torczon V, Trosset MW. A rigorous framework for optimization of expensive functions by surrogates. Structural optimization. 1999;17:1-13.
[43] Matheron G. A simple substitute for conditional expectation: the disjunctive kriging. Advanced geostatistics in the mining industry: Springer; 1976. p. 221-36.
[44] Sacks J, Welch WJ, Mitchell TJ, Wynn HP. Design and analysis of computer experiments. Statistical science. 1989:409-23.
[45] Chung DH, Kwon TH. Improved model of orthotropic closure approximation for flow induced fiber orientation. Polymer Composites. 2001;22:636-49.
[46] Chung DH, Kwon TH. Invariant-based optimal fitting closure approximation for the numerical prediction of flow-induced fiber orientation. Journal of Rheology. 2002;46:169-94.
[47] Cintra Jr JS, Tucker III CL. Orthotropic closure approximations for flow-induced fiber orientation. Journal of Rheology. 1995;39:1095-122.
[48] Hill R. Elastic properties of reinforced solids: some theoretical principles. Journal of the Mechanics and Physics of Solids. 1963;11:357-72.
[49] Greene MS, Xu H, Tang S, Chen W, Liu WK. A generalized uncertainty propagation criterion from benchmark studies of microstructured material systems. Computer Methods in Applied Mechanics and Engineering. 2013;254:271-91.
[50] Harris WM, Chiu WK. Determining the representative volume element size for three-dimensional microstructural material characterization. Part 1: Predictive models. Journal of Power Sources. 2015;282:552-61.
[51] Hong L, Wan Y, Jain A. Fingerprint image enhancement: Algorithm and performance evaluation. IEEE transactions on pattern analysis and machine intelligence. 1998;20:777-89.
[52] Kovesi P. Phase preserving tone mapping of non-photographic high dynamic range images. Digital Image Computing Techniques and Applications (DICTA), 2012 International Conference on: IEEE; 2012. p. 1-8.